Chemical Engineering Science 245 (2021) 116941

Contents lists available at ScienceDirect

Chemical Engineering Science

journal homepage: www.elsevier.com/locate/ces

C_2H_2 semi-hydrogenation on the $Pd_{shell}@M_{core}$ (M = Cu, Ag, Au) alloy catalysts: The influence of shell Pd ensemble form on the catalytic activity and selectivity

Yamin Qi [a,b,1], Xiuxiu Shao [a,b,1], Baojun Wang [a,b,*], Debao Li [c], Lixia Ling [a,b], Riguang Zhang [a,b,*]

[a] State Key Laboratory of Clean and Efficient Coal Utilization, Taiyuan University of Technology, Taiyuan 030024, Shanxi, PR China
[b] Key Laboratory of Coal Science and Technology (Taiyuan University of Technology), Ministry of Education, PR China
[c] State Key Laboratory of Coal Conversion, Institute of Coal Chemistry, Chinese Academy of Sciences, Taiyuan 030001, Shanxi, PR China

HIGHLIGHTS

- The catalytic performance of C_2H_2 semi-hydrogenation on the Pd@M catalysts strongly depends on the shell Pd ensemble form.
- Pd_7@M with the Pd ensemble of dimer and trimer exhibits the best catalytic performance toward C_2H_4 formation.
- The activity and selectivity of C_2H_4 formation has a volcano curve relationship with the *d*-band center of Pd@M catalysts.
- Pd_7@M catalysts with the best catalytic performance are attributed to the moderate *d*-band center.

GRAPHICAL ABSTRACT

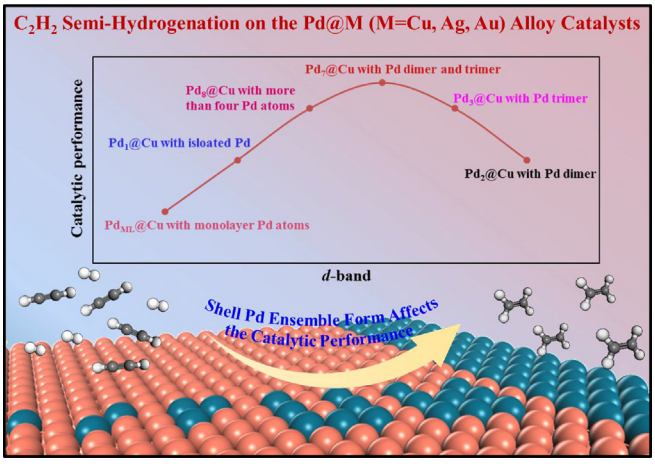

ARTICLE INFO

Article history:
Received 14 April 2021
Received in revised form 17 June 2021
Accepted 12 July 2021
Available online 14 July 2021

Keywords:
C_2H_2 semi-hydrogenation
Pd@M catalyst
Shell Pd ensemble
Catalytic performance
Electronic structure analysis

ABSTRACT

To reveal the influence of shell Pd ensemble form in the core–shell Pd@M (M = Cu, Ag, Au) catalysts on the catalytic performance of C_2H_2 semi-hydrogenation, the mechanism of C_2H_2 semi-hydrogenation on Pd@M catalysts with different shell Pd ensemble are fully investigated using DFT and microkinetic modeling calculations. The results show that C_2H_4 selectivity and its formation activity closely depend on the shell Pd ensemble form; among Pd@Cu with different shell Pd ensemble, C_2H_4 selectivity and its formation activity has a volcano curve relationship with the *d*-band center of Pd@Cu, in which Pd_7@Cu with the shell Pd ensemble of dimer and trimer is the best due to the moderate *d*-band center. The same things also occur on the Pd@Ag and Pd@Au. It is proposed that controlling the ensemble form of shell noble-metal Pd may be a good way to adjust the catalytic performance toward the selective hydrogenation of other alkynes.

* Corresponding authors at: State Key Laboratory of Clean and Efficient Coal Utilization, Taiyuan University of Technology, Taiyuan 030024, Shanxi, PR China.
E-mail addresses: wangbaojun@tyut.edu.cn (B. Wang), zhangriguang@tyut.edu.cn (R. Zhang).
[1] Represents co-first authors, and contributed equally to this work.

https://doi.org/10.1016/j.ces.2021.116941
0009-2509/

1. Introduction

One of the important chemical method to remove trace C_2H_2 impurities in C_2H_4 raw materials produced by petroleum pyrolysis is C_2H_2 semi-hydrogenation (Yang et al., 2012; Zhang et al., 2016). Pd catalyst has been widely employed in C_2H_2 semi-hydrogenation due to its excellent activity (Khan et al., 2006; Ngamsom et al., 2004). However, the high cost and the poor C_2H_4 selectivity limit its industrial application (Osswald et al., 2008). In order to solve these issues, the transition metals Au (Sárkány et al., 2008; Sárkány et al., 2002), Ag (Pei et al., 2015; Lee et al., 2011); or Cu (Leviness et al., 1984; Guczi et al., 1999) doped into Pd catalysts were used to improve C_2H_4 selectivity. Meanwhile, the metal Pd doped into the substrate Cu, Ag and Au to form PdCu (Leviness et al., 1984; Friedrich et al., 2013; McCue et al., 2014); PdAg (Pei et al., 2015; Meng and Wang, 2014; Liu, 2016; Komeili et al., 2015); and PdAu (Zhang et al., 2014) alloy catalysts are also studied for C_2H_2 semi-hydrogenation due to its better catalytic performance toward C_2H_4 formation, for instance, the experiments (McCue et al., 2014) showed that Pd-doped Cu/Al_2O_3 catalysts with Cu:Pd ratio of 50:1 exhibits 80% C_2H_4 selectivity and 90% C_2H_2 conversion at 363 K. Leviness et al. (Leviness et al., 1984) showed that the decreasing of surface Pd content on $PdCu/Al_2O_3$ at elevated temperature leads to an increase of C_2H_4 selectivity in C_2H_2 hydrogenation. Further, the Ag-based and Au-based catalysts were also investigated, for example, the experiments (Pei et al., 2015) indicated that the simultaneous high C_2H_2 conversion and C_2H_4 selectivity were attained over the single-atom Pd doped Ag alloy catalysts. Compared to Pd catalyst, Zhang et al. (Zhang et al., 2014) showed that both Ag-Pd and Au-Pd supported by SiO_2 increase C_2H_4 selectivity.

Nowadays, the core–shell catalysts presented the excellent catalytic performance due to their unique structures (McCue et al., 2014; Feng et al., 2018; Tedsree et al., 2011); for example, He et al. (He et al., 2016) demonstrated that the core–shell Cu_1Pd_3@-Pd catalyst enhanced HCOOH dissociation activity with better durability compared to Pd catalyst. The experiments (Ren et al., 2014) found that Cu@Pd/C with a Cu:Pd atomic ratio of 27:73 has the highest activity of HCOOH oxidation. Takht et al. (Takht et al., 2014) experimentally synthesized the core–shell Pd-Ag/α-AlO_3, in which Pd loaded as a shell layer of 20–30 μm thickness has 100% C_2H_4 selectivity. Sárkány et al. (Sárkány et al., 2008) synthesized Pd_{shell}-Au_{core}/SiO_2 with various thicknesses of Pd shell, the 68–80% Pd homogenized particle on Au core exhibits superior catalytic activity and selectivity for the hydrogenation reaction. Wang et al. (Wang et al., 2013) found that Au@Pd/N-mrGO shows better HCOOH dissociation activity to produce H_2 in comparison with its alloy or monometallic counterparts at room temperature. Thus, the core–shell Pd@M (M = Cu, Ag, Au) catalysts exhibit excellent performance toward some targeted reactions.

Further, the shell metal ensemble of core–shell alloy catalysts has significant influence on their catalytic performance; for example, Wang et al. (Wang et al., 2020) showed that Pd trimer of PdAg catalysts were prospective for C_2H_2 semi-hydrogenation. Ma et al. (Ma et al., 2017) theoretically indicated that 0.01 ML Pd on Pd/Cu (1 1 1) surface exhibited better C_2H_4 selectivity and its formation activity than 1.00 ML Pd in C_2H_2 semi-hydrogenation. Choi et al. (Choi et al., 2019) demonstrated that the best activity of HCOOH dissociation into H_2 was obtained on Pd@PdAg catalysts, in which PdAg alloy cores has an average Pd/Ag atomic ratio of 3.5:1 and Pd shells with 1.1 atomic layers. Zhang et al. (Zhang et al., 2018) found that Pd-modified Cu catalysts with Pd ensemble consisted of one surface and its connected subsurface Pd atoms enhance C_2H_4 selectivity and its formation activity, which is attributed to the electronic properties change of the catalyst surface. Duan et al. (Duan et al., 2016) showed that Pt_{ML}@Au(1 1 1) is highly active and selective toward HCOOH oxidation, which effectively inhibit the formation of poisonous species CO. Wang et al. (Wang et al., 2019) theoretically revealed that Pd@Au catalysts with the shell Pd dimer achieve the highest activity of CO_2 reduction. Experimental and theoretical studies by Lee et al. (Lee et al., 2016) demonstrated that Pd@Au with the shell Pd trimer exhibited the excellent catalytic performance in HCOOH dehydrogenation. Yang et al. (Yang et al., 2019) elucidated that Pd dimer has the best activity of CO oxidation at low temperature, while the tetramer outperforms the other forms at high temperature. These reported studies showed that the core–shell catalyst with the special shell metal ensemble can exhibit the excellent catalytic performance. However, up to now, to the best of our knowledge, for the core–shell Pd_{shell}@M_{core} (M = Cu, Ag, Au) alloy catalysts denoted as Pd@M in this study, a fundamental understanding about the influences of the shell Pd ensemble form on C_2H_4 selectivity and its formation activity in C_2H_2 semi-hydrogenation is still ambiguous, which is of very significance to design the newly-efficient core–shell Pd@M catalyst in C_2H_2 semi-hydrogenation.

In this study, the core–shell Pd@M (M = Cu, Ag, Au) catalysts with different forms of shell Pd ensemble are designed to elucidate the influence of the shell Pd ensemble form on C_2H_4 selectivity and its formation activity in C_2H_2 semi-hydrogenation, the density functional theory (DFT) and microkinetic modeling calculations are used to probe into the underlying mechanism of C_2H_2 semi-hydrogenation on Pd@M catalysts. Further, the electronic properties are analyzed to reveal the microscopic essences. The results are expected to deepen the understanding about the influence of shell noble metal ensemble form in the core–shell catalysts on C_2H_4 selectivity and its formation activity in C_2H_2 semi-hydrogenation, and give out a valuable structure clue to design the high-efficiency core–shell catalysts that are consisted of the shell noble metal-doped into the core non-noble metal.

2. Computational details

2.1. Computational method

Dmol^3 program package of Materials Studio 8.0 were employed in all calculations in this study (Delley, 2000; Delley, 1990). Generalized gradient approximation (GGA) with the exchange–correlation functional Perdew-Burke-Ernzerhof (PBE) was implemented to calculate the electronic structure (Delley, 1996; Tian et al., 2007). The energy, maximum force and maximum displacement convergence criteria correspond to the values of 2.0×10^{-5} Ha, 4.0×10^{-3} Ha/Å and 5.0×10^{-3} Å, respectively. The cutoff values of Pd, Cu, Ag and Au elements were 4.0 Å. The smearing width was 0.005 Ha. The H and C_2H_x species were treated using all electron basis set; the Cu and Pd atoms were treated using the effective core potential (ECP) (Dolg et al., 1987). A double-valued base plus polarization function (DNP) was used to treat the valence election wave function (Zhou et al., 2007). The Brillouin zone *k*-point was selected as ($2 \times 2 \times 1$). The Complete LST/QST method was used to search transition state (Halgren and Lipscomb, 1977; Govind et al., 2003; Paul and Sautet, 1994), and confirmed by the TS Confirmation and frequency analysis.

Previous studies revealed that the high ratio of H_2/C_2H_2 and the high temperature promote C_2H_2 hydrogenation instead of its polymerization (Wehrli et al., 1991; Ahn et al., 2007; Battiston et al., 1982), meanwhile, C_2H_2 semi-hydrogenation usually happens at the temperature 300–500 K, thus, the temperature 425 K was considered for the energy calculations (the details are presented in the Supplementary Material).

2.2. Computational models

Previous experiments (Ren et al., 2014; Lu et al., 2012) demonstrated that Pd@Cu particle exhibited a narrow size range between 1.9 and 4.5 nm, and the (1 1 1) surfaces of Pd and Pd@Cu were detected by XRD pattern (Ren et al., 2014), indicating that the shell surface structure around the reactive site is similar to the periodic model, so the periodic model can be used to simulate the structural characteristics of large particles. Further, theoretical studies by He et al. (He et al., 2016) constructed $Cu_1@Pd_3$(1 1 1) periodic model to model the core–shell catalysts, and the same kinds of core–shell catalysts are also used by Yuan et al. (Yuan and Liu, 2013) and Cho et al. (Cho et al., 2017). Thus, the periodic model of M and Pd@M (M = Cu, Ag, Au) catalysts employed to present the core–shell catalysts in this study is reasonable.

For the pure metal M (M = Cu, Ag, Au) catalysts, the flat (1 1 1) surface is the mostly exposed and the most stable for the face centered cubic metal M (Eren et al., 2016; Brandt et al., 2009; Meier and Castellani, 2017), the M(1 1 1) surface with a four-layer p (4×4) unit cell is usually to model the pure metal M catalyst; the bottom one layer is fixed with the other fragments relaxed. A vacuum of 15 Å is considered to eliminate the layer-to-layer unphysical interaction between surface slabs due to the periodic images. The reliability of $p(4 \times 4)$ unit cell is also confirmed, as presented in the Supplementary Material.

Aiming at revealing the influence of shell Pd ensemble form on C_2H_4 selectivity and its formation activity in C_2H_2 semi-hydrogenation, the core–shell Pd@M (M = Cu, Ag, Au) catalysts with different forms of shell Pd ensemble are constructed with the replacement of 1, 2, 3, 7, 8 and a monolayer (16) M atoms by the corresponding number of Pd atoms, denoted as $Pd_1@M$, $Pd_2@M$, $Pd_3@M$, $Pd_7@M$, $Pd_8@M$ and $Pd_{ML}@M$, as shown in Fig. 1. Previous studies reported that these models were reliable to model different forms of shell Pd ensemble in the core–shell catalysts (Wang et al., 2019; Lee et al., 2016; Yang et al., 2019), in which the $Pd_1@M$, $Pd_2@M$ and $Pd_3@M$ catalysts are established to model the single-atom Pd, Pd dimer and Pd trimer. Moreover, previous studies by Wang et al. (Wang et al., 2020) also showed that $Pd_7@M$ and $Pd_8@M$ catalysts are established on the basis of Pd dimer and Pd trimer. Meanwhile, the experiments (Wang et al., 2019) have synthesized Pd@Au catalysts with various Pd dispersions by low temperature reduction of a palladium salt with hydrogen, in which the decoration of Au nanoparticles with Pd atoms can be obtained by precisely controlling the doses and varying the average size of Pd ensembles on the bimetallic surfaces. Similarly, the specific Pd shell ensemble catalyst used in this study could be prepared by the experiments.

3. Results and discussion

3.1. Reaction pathway of C_2H_2 semi-hydrogenation

The possible hydrogenation process in C_2H_2 semi-hydrogenation is described in Fig. 2 with three paths. The desired C_2H_4 desorption path to gas phase C_2H_4 is $C_2H_2(ad) + H(ad) \rightarrow C_2H_3(ad) + H(ad) \rightarrow C_2H_4(ad) \rightarrow C_2H_4(g)$; C_2H_4 hydrogenation path to ethane is $C_2H_2(ad) + H(ad) \rightarrow C_2H_3(ad) + H(ad) \rightarrow C_2H_4(ad) + 2H(ad) \rightarrow C_2H_6(g)$; $CHCH_3$ hydrogenation path to ethane is $C_2H_2(ad) + H(ad) \rightarrow C_2H_3(ad) + H(ad) \rightarrow CHCH_3(ad) + 2H(ad) \rightarrow C_2H_6(g)$. On the other hand, the polymerization process to produce 1,3-butadiene as the green oil precursor also includes three paths: the first is $C_2H_2(ad) + C_2H_2(ad) \rightarrow C_4H_4(ad)$; the second is $C_2H_2(ad) + C_2H_3(ad) \rightarrow C_4H_5(ad)$; the third is $C_2H_3(ad) + C_2H_3(ad) \rightarrow C_4H_6(ad)$.

Aiming at obtaining the dominant path of the hydrogenation process on the Pd@M (M = Cu, Ag, Au) catalysts, firstly, the priority between C_2H_4 desorption and its hydrogenation needs to be judged, if it is true, C_2H_4 desorption path is favored instead of C_2H_4 hydrogenation path; Then, to confirm whether C_2H_4 desorption path is also dominant compared to $CHCH_3$ hydrogenation path, if it is true, C_2H_4 desorption path is the dominant path among three paths in the hydrogenation process. Further, the polymerization process to form 1,3-butadiene is examined on the catalysts with C_2H_4 desorption path as the dominant path.

3.2. C_2H_2 and C_2H_4 adsorption on the Pd@Cu catalysts

Industrially, C_2H_2 content is 0.1–1% and C_2H_4 content is high as 89% in the raw C_2H_4 (Yang et al., 2013; Huang et al., 2007; Vincent and Gonzalez, 2004), thus, to ensure the trace C_2H_2 hydrogenation to produce C_2H_4, C_2H_2 adsorption ability must surpasses C_2H_4 adsorption ability (Zhao et al., 2018; McCue et al., 2016). The most stable adsorption structures of H and C_2H_x species on different kinds of Pd@Cu is depicted in Fig. 3, and the adsorption free energy is listed in Table S1.

C_2H_2 is stabilized at the hcp site on the $Pd_3@Cu$, $Pd_7@Cu$ and $Pd_{ML}@Cu$ catalysts with the adsorption free energies of −98.1, −86.8 and −155.0 kJ·mol^{-1}; on the $Pd_1@Cu$, $Pd_2@Cu$ and $Pd_8@Cu$ catalysts, C_2H_2 is stabilized at the sites consisted of the hcp and fcc sites via the C_{hcp}-C_{fcc} configuration with the adsorption free

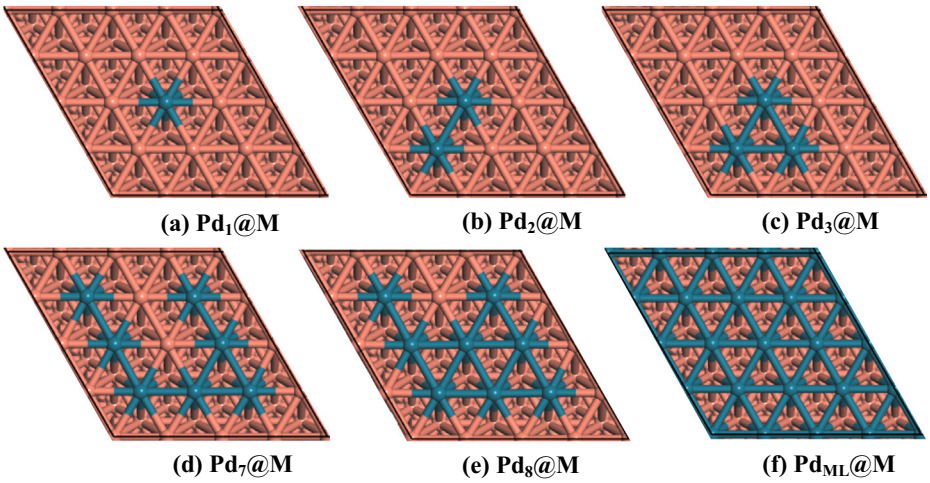

Fig. 1. The surface structure of Pd@M (M = Cu, Ag, Au) alloy catalysts, (a) $Pd_1@M$, (b) $Pd_2@M$, (c) $Pd_3@M$, (d) $Pd_7@M$, (e) $Pd_8@M$ and (f) $Pd_{ML}@M$.

(1) Hydrogenation process

$$① \ C_2H_2(ad) \xrightarrow{+H} C_2H_3(ad) \xrightarrow{+H} C_2H_4(ad) \xrightarrow{\text{desorption}} C_2H_4(g)$$

$$② \ C_2H_2(ad) \xrightarrow{+H} C_2H_3(ad) \xrightarrow{+H} C_2H_4(ad) \xrightarrow{+H} C_2H_5(ad)$$

$$③ \ C_2H_2(ad) \xrightarrow{+H} C_2H_3(ad) \xrightarrow{+H} CHCH_3(ad) \xrightarrow{+H} C_2H_5(ad)$$

(2) Polymerization process

$$① \ C_2H_2(ad) \xrightarrow{+C_2H_2} C_4H_4(ad)$$

$$② \ C_2H_2(ad) \xrightarrow{+H} C_2H_3(ad) \xrightarrow{+C_2H_2} C_4H_5(ad)$$

$$③ \ C_2H_2(ad) \xrightarrow{+H} C_2H_3(ad) \xrightarrow{+C_2H_3} C_4H_6(ad)$$

Fig. 2. Possible reactions in the hydrogenation and polymerization processes of C_2H_2 semi-hydrogenation. The (ad) and (g) stand for the adsorbed and gaseous states, respectively.

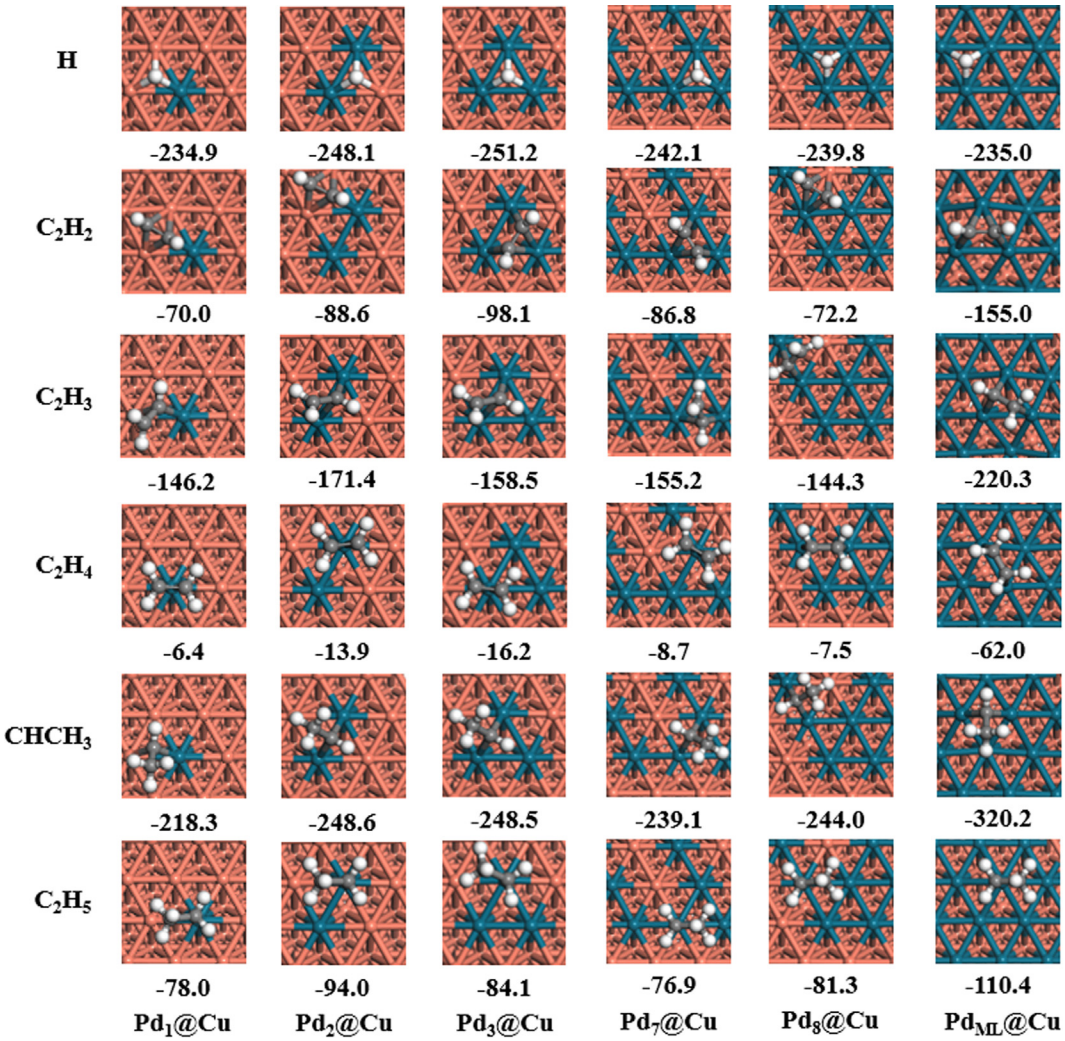

Fig. 3. The most stable adsorption configurations and the corresponding adsorption free energy ($kJ \cdot mol^{-1}$) of H and C_2H_x(x = 2–5) adsorbed on the Pd@Cu catalysts at 425 K.

energies of −70.0, −88.6 and −72.2 kJ·mol^{-1}, respectively. C_2H_4 prefers to adsorb at the bridge site on the Pd_8@Cu and Pd_{ML}@Cu, and that is at the top site on the Pd_1@Cu, Pd_2@Cu, Pd_3@Cu and Pd_7@Cu; the adsorption free energies are −7.5, −62.0, −6.4, −13.9, −16.2 and −8.7 kJ·mol^{-1}, respectively; Namely, expect for Pd_{ML}@Cu, once the shell Pd ensemble is formed, C_2H_4 adsorption becomes weaker on the Pd_1@Cu, Pd_2@Cu, Pd_3@Cu, Pd_7@Cu and Pd_8@Cu, which is favorable for C_2H_4 desorption. Thus, C_2H_2 has stronger adsorption ability than C_2H_4 on the six kinds of Pd@Cu catalysts, the trace C_2H_2 in the raw C_2H_4 material can be sufficiently adsorbed on the catalysts for C_2H_2 semi-hydrogenation.

For the other adsorbed species, the adsorption free energy is in sequence of $CHCH_3$ > C_2H_3 > C_2H_5 on Pd@Cu catalysts, the adsorption energies of these species are insensitive to the shell Pd ensemble. H adsorption free energy is in the range of −234.9 to −251.2 kJ·mol^{-1}, which also less depend on the shell Pd ensemble.

3.3. C_2H_2 semi-hydrogenation on the Pd@Cu catalysts

In C_2H_2 semi-hydrogenation, for the activation free energy of the adsorbed reactants, previous works by Hu *et al.* (Yang et al., 2013; Cao et al., 2011; Yang et al., 2014) proposed that the transition-state of adsorption process has lower energy than the total energy of the gas phase species. Thus, the maximum adsorption barrier of the species R corresponds to the value of TS_R (R = C_2H_2 or H_2), where S_R is the corresponding entropy of the species R at the reaction temperature *T*. Moreover, the value of TS_{C2H2} is higher than that of TS_{H2}, namely, C_2H_2 adsorption has the higher barrier. Further, the value of TS_{C2H2} is selected to represent the adsorption activation free energy of the reactants (*G*ad R).

In this study, the values of TS_{C2H2} and TS_{H2} were calculated to be 92.0 and 59.9 kJ·mol^{-1} at 425 K, respectively. Namely, C_2H_2 adsorption still has the higher adsorption barrier, which agree with the previous studies by Hu et al. (Yang et al., 2013; Cao et al., 2011; Yang et al., 2014). Thus, the adsorption barrier of the reactants on Pd@Cu catalysts is represented by the adsorption barrier of C_2H_2 (92.0 kJ·mol^{-1}). On the other hand, the overall reaction free energy of C_2H_2 hydrogenation to C_2H_4 is −206.3 kJ·mol^{-1} at 425 K obtained from DFT calculations. Therefore, the activation free energy of the adsorbed reactants and the entropy effect are considered for the adsorption and desorption processes.

Nowadays, the previous studies by Hu et al. (Yang et al., 2013; Yang et al., 2012; Yang et al., 2014; Yang et al., 2016; Yang et al., 2017), Mavrikakis et al. (Xu et al., 2018), Celik et al. (Hook and Celik, 2017), Hafner et al. (Krajčí and Hafner, 2014), Kang et al. (Zhao et al., 2018), Wang et al. (Ma and Wang, 2020) and Gong et al. (Zhao et al., 2019) have proposed the simplest descriptor when $CHCH_3$ hydrogenation path is not the dominant path, that is the energy difference between C_2H_4 desorption and its hydrogenation to quantitatively and qualitatively evaluate C_2H_4 selectivity. Meanwhile, C_2H_4 desorption free energy is approximately equal to its adsorption free energy (Cao et al., 2011). Thus, C_2H_4 selectivity (S_{sel}) is defined as follows:

$$S_{sel} = G_{a,hydr} - G_{a,des} = G_{a,hydr} - |G_{ads}| \quad (1)$$

where $G_{a,hydr}$ corresponds to the activation free energy of the reaction C_2H_4 + H → C_2H_5, $G_{a,des}$ is the adsorption free energy of C_2H_4 desorption; the better C_2H_4 selectivity corresponds to the more positive value of S_{sel}.

3.3.1. On Pd_1@Cu catalyst

As depicted in Fig. 4 and Table 1, starting with the gas phase reactants, the adsorption and desorption processes consider the activation of the adsorbed reactants and the entropy effect in the C_2H_2 semi-hydrogenation. C_2H_4 desorption is more favorable than C_2H_4 hydrogenation in kinetics (6.4 *vs.* 86.1 kJ·mol^{-1}, S_{sel} = 79.7 kJ·mol^{-1}), C_2H_4 desorption path becomes dominant compared to C_2H_4 hydrogenation path. Then, the reaction C_2H_3(ad) + H(ad) → CHCH_3(ad) is kinetically difficult to occur compared to the reaction C_2H_3(ad) + H(ad) → C_2H_4(ad) (124.8 *vs.* 54.6 kJ·mol^{-1}), that is, C_2H_4 desorption path is kinetically favored compared to $CHCH_3$ hydrogenation path. Further, the activation free energy of C_2H_2(ad) + H(ad) → C_2H_3(ad) is 138.5 kJ·mol^{-1} with the reaction free energy of −39.8 kJ·mol^{-1}. The activation free energy of C_2H_2(g) + H_2(g) → C_2H_2(ad) + 2H(ad) is 92.0 kJ·mol^{-1} with the reaction free energy of −84.1 kJ·mol^{-1}. Thus, C_2H_2 hydrogenation on Pd_1@Cu dominantly contributes to gas phase C_2H_4 formation via the desorption route.

3.3.2. On the Pd_2@Cu, Pd_3@Cu, Pd_7@Cu and Pd_8@Cu catalysts

As depicted in Figs. S3–S6, similar to Pd_1@Cu catalyst, C_2H_4 desorption path to produce gas phase C_2H_4 is the most favorable kinetically than other two paths on the Pd_2@Cu, Pd_3@Cu, Pd_7@Cu and Pd_8@Cu catalysts, correspondingly, C_2H_4 selectivity is 81.2, 87.9, 151.0 and 75.4 kJ·mol^{-1}, respectively. Thus, the Pd_2@Cu, Pd_3@Cu, Pd_7@Cu and Pd_8@Cu catalysts are in favor of C_2H_2 hydrogenation to produce gas phase C_2H_4 instead of ethane via other two paths.

3.3.3. On Pd_{ML}@Cu catalyst

As depicted in Fig. 5, C_2H_4 desorption is more kinetically favorable than the reaction C_2H_4 + H → C_2H_5 (62.0 *vs.* 87.5 kJ·mol^{-1}), however, C_2H_3 + H → $CHCH_3$ is more kinetically superior to C_2H_3 + H → C_2H_4 (110.7 *vs.* 126.9 kJ·mol^{-1}); moreover, with respect to the common C_2H_3 + H species, $CHCH_3$ hydrogenation path is more favored in kinetics compared to C_2H_4 desorption path (−66.9 *vs.* −50.7 kJ·mol^{-1}). Thus, $CHCH_3$ hydrogenation path becomes dominant, which affects C_2H_4 selectivity on Pd_{ML}@Cu catalyst, C_2H_4 selectivity is −16.2 kJ·mol^{-1}, which is calculated by the descriptor that is the difference of the overall energy between $CHCH_3$ hydrogenation path and C_2H_4 desorption path beginning with the common C_2H_3 + H species.

3.4. Activity of C_2H_4 formation on the Pd@Cu catalysts

Hu et al. (Yang et al., 2013; Cao et al., 2011; Yang et al., 2014; Cheng and Hu, 2011; Cheng et al., 2008) have proposed the two-step model to describe the activity of C_2H_4 formation, which is calculated by the Eq. (2) (see details in the Supplementary Material).

$$r = \frac{k_B T}{h} = \frac{\left(1 - \frac{P_P}{P_R} e^{\frac{\Delta G}{RT}}\right)}{\frac{P^0}{P_R} e^{\frac{G_R^{ad} - G_R^{de} + G_P^{de}}{RT}} + e^{\frac{G_P^{de}}{RT}}} \quad (2)$$

As listed in Table 2, Pd_{ML}@Cu exhibits the lowest activity of C_2H_4 formation (3.06 × 10^{-6} s^{-1}·site^{-1}), while for the Pd_1@Cu, Pd_2@Cu, Pd_3@Cu and Pd_7@Cu catalysts, with the increasing of alloyed shell Pd atoms, both Pd dimer and Pd trimer are formed on the catalyst surface, the activity of C_2H_4 formation gradually increased (8.40 × 10^{-5}, 2.17 × 10^{3}, 6.29 × 10^{4} and 5.66 × 10^{6} s^{-1}·site^{-1}). However, when the shell Pd atoms increase to form Pd_8@Cu, the activity of C_2H_4 formation decreased to 9.27 × 10^{2} s^{-1}·site^{-1}. Among these six catalysts, Pd_7@Cu with the shell Pd ensemble of both Pd dimer and trimer exhibits the highest activity of C_2H_4 formation (5.66 × 10^{6} s^{-1}·site^{-1}).

3.5. General discussion

3.5.1. The influence of the shell Pd ensemble form on C_2H_4 formation

Based on above analysis, C_2H_4 selectivity is in sequence of Pd_7@Cu > Pd_3@Cu > Pd_2@Cu > Pd_1@Cu > Pd_8@Cu > Pd_{ML}@Cu (151.0, 87.9, 81.2, 79.7, 75.4 and −16.2 kJ·mol^{-1}). Correspondingly, C_2H_4 formation rates follows the order of Pd_7@Cu > Pd_3@Cu > Pd_2@-

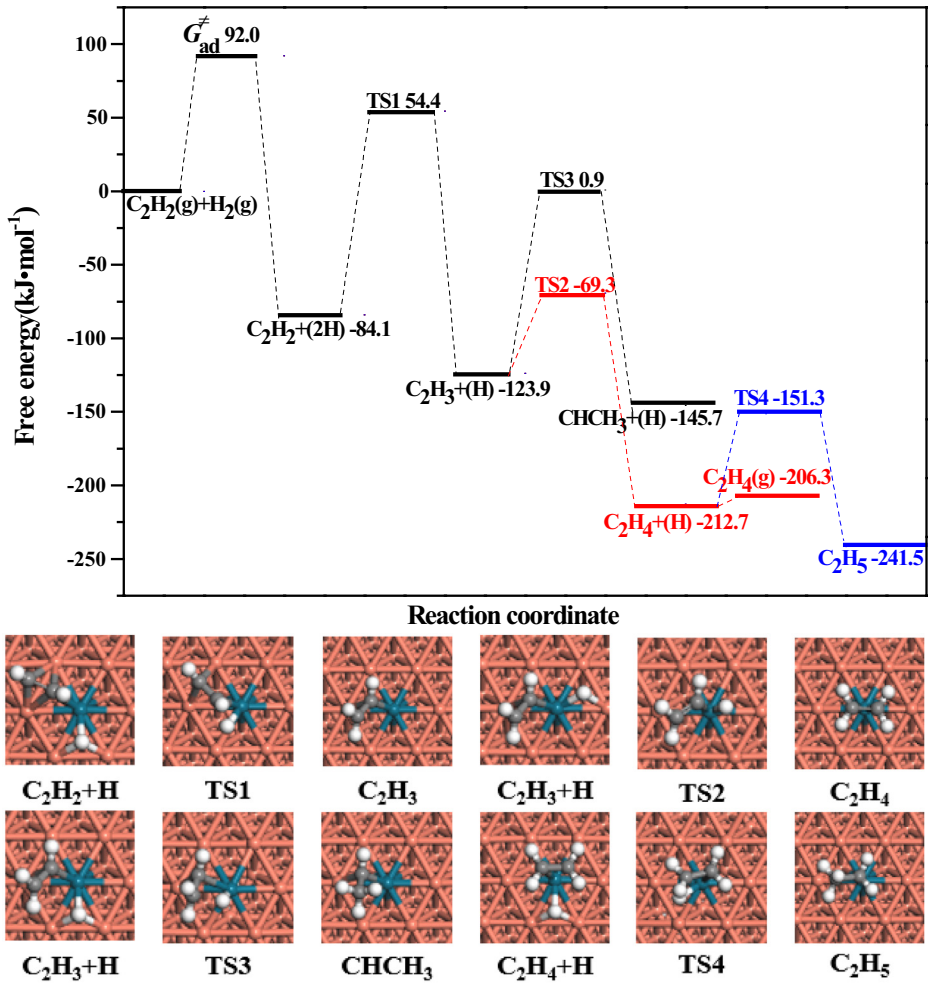

Fig. 4. Free energy profiles of C_2H_2 semi-hydrogenation with the initial states, transition states and final states on Pd_1@Cu catalyst.

Table 1
The activation free energy (reaction free energy) (kJ·mol^{-1}) of C_2H_2 semi-hydrogenation on the Pd@M (M = Cu, Ag, Au) alloy catalysts.

Catalysts	Elementary reactions				
	C_2H_2 + H → C_2H_3	C_2H_3 + H → C_2H_4	C_2H_3 + H → $CHCH_3$	C_2H_4 + H → C_2H_5	$CHCH_3$ + H → C_2H_5
Pd_1@Cu	138.5(−39.8)	54.6(−88.8)	124.8(−21.8)	86.1(−28.8)	–
Pd_2@Cu	78.2(−44.2)	73.3(−67.2)	225.6(−15.2)	95.1(−16.2)	–
Pd_3@Cu	66.3(−14.5)	49.7(−74.2)	221.7(−19.8)	104.1(−1.7)	–
Pd_7@Cu	50.4(−59.9)	68.5(−77.2)	229.5(−20.8)	159.7(5.0)	–
Pd_8@Cu	81.2(−36.6)	83.0(−80.0)	196.1(−29.7)	82.9(−8.9)	–
Pd_{ML}@Cu	84.4(23.3)	126.9(−90.7)	110.7(−57.6)	87.5(−3.4)	160.3(−15.9)
Pd_7@Ag	50.7(−28.6)	83.3(−51.6)	119.4(3.6)	90.0(5.5)	–
Pd_{ML}@Ag	103.7(31.0)	100.2(−22.3)	254.1(4.7)	169.8(40.5)	103.9(7.0)
Pd_7@Au	61.9(−8.7)	85.2(−43.3)	197.6(−12.4)	75.2(−10.5)	–
Pd_{ML}@Au	83.6(30.5)	118.5(−17.0)	258.0(14.0)	110.6(35.8)	135.7(8.8)

Cu > Pd_8@Cu > Pd_1@Cu > Pd_{ML}@Cu (5.66×10^6, 6.29×10^4, 2.17×10^3, 9.27×10^2, 8.40×10^{-5} and 3.06×10^{-6} s^{-1}·$site^{-1}$).

As depicted in Fig. 1, the shell surface structure of Pd@Cu catalysts showed that Pd_1@Cu, Pd_2@Cu and Pd_3@Cu have the surface isolated Pd atom, Pd dimer, and Pd trimer, respectively; Pd_7@Cu has both the surface Pd dimer and trimer. While Pd_{ML}@Cu without the surface Pd dimer and trimer present the surface characteristic of the pure Pd. Pd_8@Cu catalyst with more than four Pd atoms polymers has poor C_2H_4 formation activity. Among them, Pd_2@Cu with the shell Pd dimer and Pd_3@Cu with the shell Pd trimer exhibit excellent C_2H_4 selectivity and its formation activity, especially, Pd_7@Cu with the shell Pd dimer and trimer shows the best C_2H_4 selectivity and its formation activity.

Further, as depicted in Fig. 3, the most stable adsorption site of both H and C_2H_x(x = 2–5) on Pd@Cu catalysts is at the Pd-Cu interface site near the Pd dimer and trimer. Moreover, the initial state (IS), transition state (TS) and final state (FS) are almost adsorbed at the Pd dimer on Pd_2@Cu. Similarly, the IS, TS and FS prefer to be located at the Pd trimer on Pd_3@Cu. Especially, for the Pd_7@Cu and Pd_8@Cu, the IS, TS and FS are located at the Pd-Cu interface site near the Pd dimer and trimer.

Based on the above analysis, the existence forms of shell Pd ensemble obviously affect C_2H_4 selectivity and its formation activity on Pd@Cu catalysts; meanwhile, there must be a synergy between Pd and Cu atoms near the shell Pd dimer and trimer to increase C_2H_4 selectivity and its formation activity.

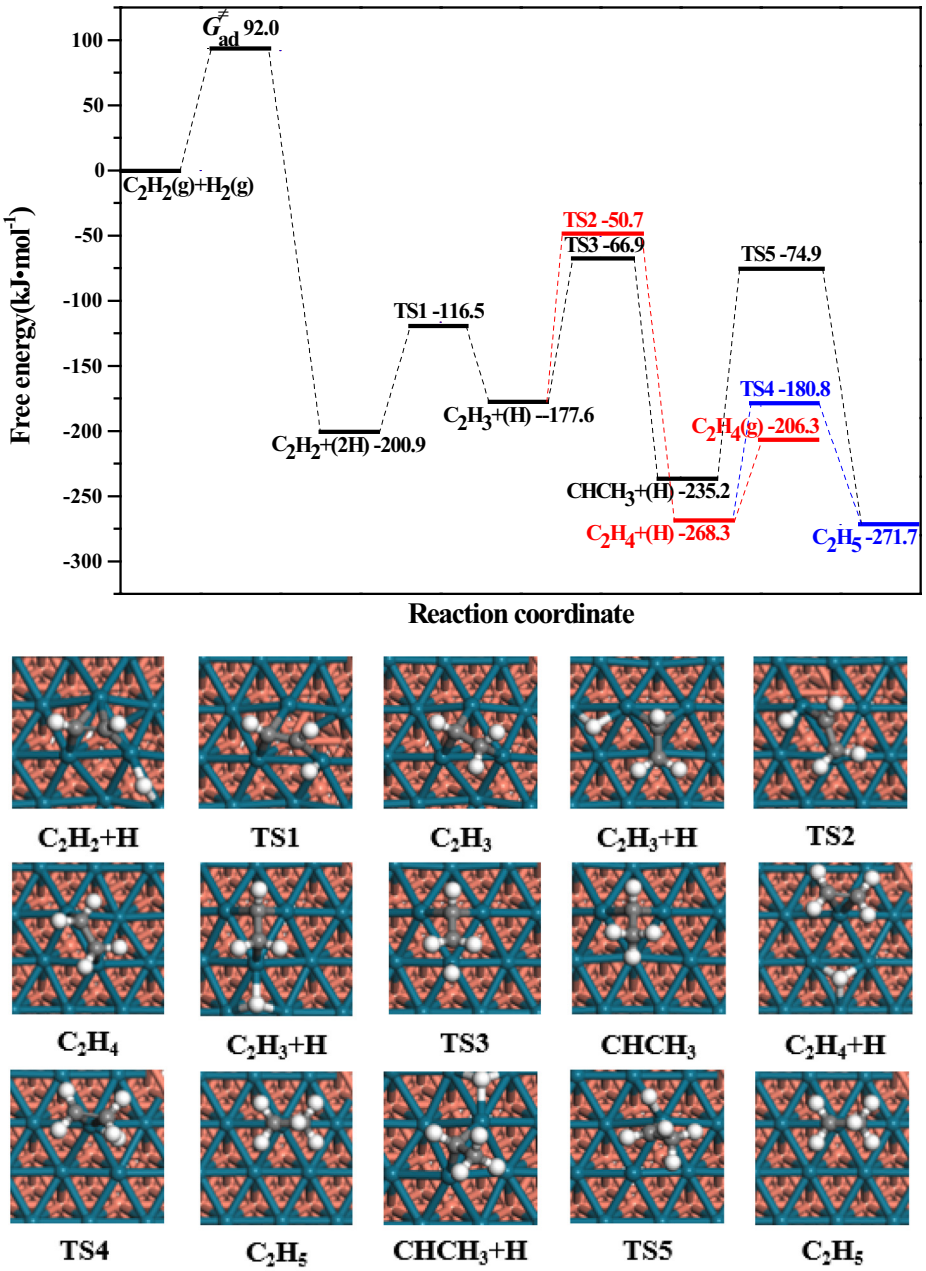

Fig. 5. Free energy profiles of C_2H_2 semi-hydrogenation with the initial states, transition states and final states on Pd_{ML}@Cu catalyst.

Table 2
The values of C_2H_4 selectivity (S_{sel}/kJ·mol^{-1}), formation rate (r/s^{-1}·site^{-1}) and the average Bader charge (e) obtained by the surface Pd atoms on the Pd@M (M = Cu, Ag, Au) alloy catalysts.

Catalysts	S_{sel}	r	e
Pd_1@Cu	79.7	8.40×10^{-5}	0.941
Pd_2@Cu	81.2	2.17×10^{3}	0.944
Pd_3@Cu	87.9	6.29×10^{4}	0.949
Pd_7@Cu	151.0	5.66×10^{6}	0.847
Pd_8@Cu	75.4	9.27×10^{2}	0.870
Pd_{ML}@Cu	−16.2	3.06×10^{-6}	0.748
Pd_7@Ag	71.8	1.68×10^{6}	0.958
Pd_{ML}@Ag	143.6	1.02×10^{-9}	0.749
Pd_7@Au	47.8	3.50×10^{3}	0.999
Pd_{ML}@Au	74.5	4.30×10^{-6}	0.749

3.5.2. Electronic properties analysis of Pd@Cu catalysts

To better clarify the influences of Pd@Cu with different forms of shell Pd ensemble on C_2H_4 selectivity and its formation activity, a projected density of states (*p*DOS) and *d*-band center of Pd@Cu catalysts was conducted to explain the microscopic essence, see Fig. S12, the *d*-band center of Pd@Cu with different forms of shell Pd ensemble is in the sequence of Pd_{ML}@Cu (−2.501) < Pd_1@Cu (−2.500) < Pd_8@Cu (−2.493) < Pd_7@Cu (−2.487) < Pd_3@Cu (−2.443) < Pd_2@Cu (−2.429).

As depicted in Fig. 6a and b, the *d*-band center of the shell Pd atoms and their coordinated Cu atoms has a volcano curve relationship with C_2H_4 selectivity and its formation activity on Pd@Cu catalysts, namely, the *d*-band center of both Pd_{ML}@Cu and Pd_1@Cu shifts away compared to the Fermi level, which exhibits the lower C_2H_4 selectivity and formation activity; whereas the *d*-band center of both Pd_2@Cu and Pd_3@Cu with the shell Pd ensemble of dimer

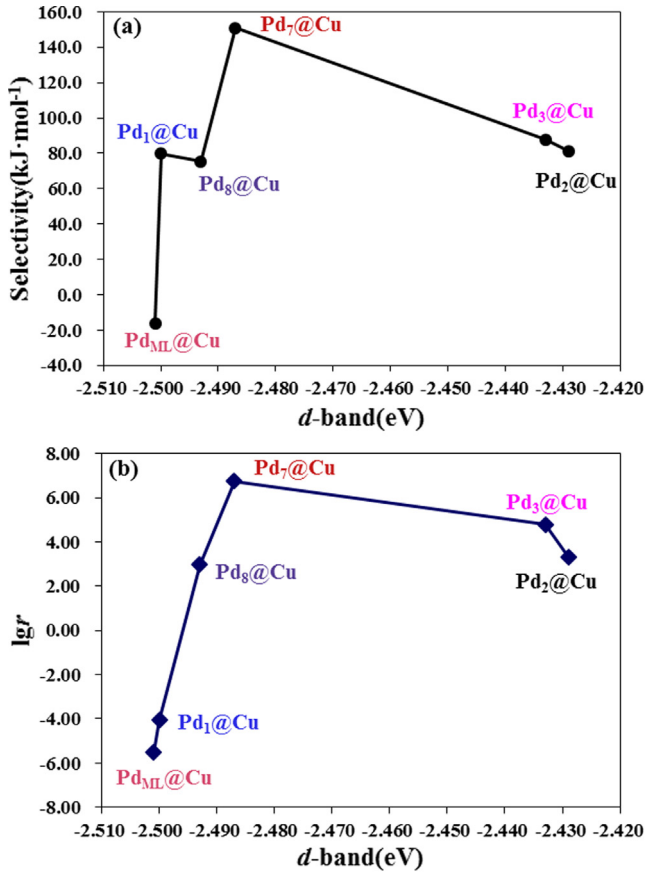

Fig. 6. The relationship between the selectivity of C_2H_4 (kJ·mol^{-1}) and *d*-band center (a), that between the formation rate of C_2H_4 (lgr/s^{-1}·site^{-1}) and *d*-band center (b) on the Pd@Cu catalysts.

and trimer shifts toward the Fermi level, exhibiting better catalytic performance. Interestingly, Pd_7@Cu catalyst with the moderate *d*-band center presents the best C_2H_4 selectivity and its formation activity, which may be attributed to the special surface geometry structure that is the shell Pd ensemble with both Pd dimer and Pd trimer. Thus, the existence form of shell Pd ensemble alters the *d*-orbital distribution of Pd@Cu catalysts, and the synergetic interaction of electronic properties and geometry structure affects the catalytic performance of Pd@Cu catalysts in C_2H_2 semi-hydrogenation; Namely, the catalytic performance not only depends on the *d*-band center of the active center but also depends on the shell Pd ensemble forms. In addition, previous studies (Liu et al., 2013; Deng et al., 2020; Ando et al., 2018; Fu et al., 2020; Song et al., 2019) also demonstrated that the catalytic activity has a volcano curve relationship with the *d*-band center of the catalysts, and the catalyst with a moderate *d*-band center exhibits the best catalytic performance, which is attributed to that the adsorption ability of the adsorbed species have a close correlation with the *d*-band center, suggesting that the farther the *d*-band center of the catalyst surface from the Fermi level is, the stronger the adsorption ability of the species on the catalysts is; when the adsorption ability is too strong, the adsorbed species is difficult to participate into the reaction, whereas the adsorption ability is too weak, the adsorbed species cannot be effectively activated, and it is difficult to initiate the subsequent reaction; thus, a moderate adsorption ability is more beneficial for the adsorbed species to initiate the subsequent reaction.

Based on the above analysis, a moderate *d*-band center shows excellent catalytic performance. As presented in Fig. 3, the relationship between the adsorption energy of adsorbed species and the *d*-band is also roughly the same trend. The moderate adsorption ability of C_2H_2 on Pd_7@Cu catalyst is conducive to its hydrogenation and shows high C_2H_4 formation activity; and the moderate adsorption ability of C_2H_4 is beneficial to its desorption and present better C_2H_4 selectivity.

On the other hand, the average Bader charge of shell Pd atoms is examined, see Table 2; the charge density difference of Pd@Cu is also considered, as depicted in Fig. 7, correspondingly, the average Bader charge of the shell Pd atoms decreases in sequence of Pd_3@Cu (0.949 *e*) > Pd_2@Cu (0.944 *e*) > Pd_1@Cu (0.941 *e*) > Pd_8@Cu (0.870 *e*) > Pd_7@Cu (0.847 *e*) > Pd_{ML}@Cu (0.748 *e*). Meanwhile, the charge density differences in Fig. 7a–f shows that the electron accumulation decreases at the region of Pd atoms with the decreasing of the average Bader charge of the shell Pd atoms. Thus, both Pd_1@Cu and Pd_{ML}@Cu catalysts at the region of Pd atoms corresponding to most and least electron accumulation have the lowest catalytic performance. Although the region of Pd atoms of Pd_3@Cu and Pd_2@Cu corresponds to the most electron accumulation, both catalysts present better catalytic performance, which is probably attributed to the shell Pd ensemble form. Pd_7@Cu catalyst at the region of Pd atoms with moderate electron accumulation exhibits the excellent catalytic performance toward C_2H_2 semi-hydrogenation.

Generally, Pd_7@Cu with the shell Pd ensemble of dimer and trimer presents the best C_2H_4 selectivity and its formation activity. Thus, it is proposed that this type of catalysts with the shell Pd ensemble of dimer and trimer can be also applied to other kinds of Pd@M catalysts in C_2H_2 semi-hydrogenation.

3.5.3. The influence of shell Pd ensemble in Pd@M (M = Ag, Au) on C_2H_4 formation

Similar to Pd@Cu catalysts, aiming at confirming whether other metal core with the shell Pd ensemble of dimer and trimer still favor C_2H_4 formation with high selectivity and activity, C_2H_2 semi-hydrogenation on the Pd_7@M and Pd_{ML}@M (M = Ag, Au) catalysts were considered (see details in the Supplementary Material).

C_2H_2 adsorption is still much stronger than C_2H_4 adsorption on the Pd_7@Ag, Pd_{ML}@Ag, Pd_7@Au and Pd_{ML}@Au (see Table S1 and Fig. S7). As depicted in Figs. S8–S11, the formation of gas phase C_2H_4 via C_2H_4 desorption path is kinetically favored compared to other two hydrogenation paths to form ethane on the Pd_7@Ag, Pd_{ML}@Ag, Pd_7@Au and Pd_{ML}@Au, correspondingly, C_2H_4 selectivity is 71.8, 143.6, 47.8 and 74.5 kJ·mol^{-1}, the formation rates are 1.68×10^6, 1.02×10^{-9}, 3.50×10^3 and 4.30×10^{-6} s^{-1}·site^{-1}, respectively. Previously reported works by Wang et al. (Wang et al., 2020) found that C_2H_4 hydrogenation to C_2H_5 is energetically comparable to its desorption over Pd_2@Ag with Pd dimer (44.3 *vs.* 47.1 kJ·mol^{-1}), showing a poor C_2H_4 selectivity, meanwhile, Pd_3@Ag with Pd trimer exhibits better catalytic performance toward C_2H_4 formation (S_{sel} = 44.7 kJ·mol^{-1}, $r = 7.11 \times 10^3$ s^{-1}·site^{-1}); thus, Pd_7@Ag shows the best catalytic activity and selectivity toward C_2H_4 formation among Pd@Ag catalysts.

Markedly, both Pd_7@Ag and Pd_7@Au with the shell Pd ensemble of dimer and trimer exhibit better C_2H_4 formation activity compared to Pd_{ML}@Ag and Pd_{ML}@Au catalysts with a whole layer of surface Pd. Moreover, the average charge of the shell Pd atoms for Pd_7@Ag catalyst is more than that of Pd_{ML}@Ag (0.958 *e vs.* 0.749 *e*), similarly, the average charge of the shell Pd atoms for Pd_7@Au is more than that of Pd_{ML}@Au (0.999 *e vs.* 0.749 *e*), which is also confirmed by the charge density difference, see Fig. 7g–j.

3.5.4. The influence of the core metal type for Pd_7@M catalysts on C_2H_4 formation

As mentioned above, among Pd_7@M (M = Cu, Ag, Au) catalysts, Pd_7@Cu presents the highest C_2H_4 formation activity (5.66×10^6 *vs.* 1.68×10^6, 3.50×10^3 s^{-1}·site^{-1}) and the best C_2H_4 selectivity

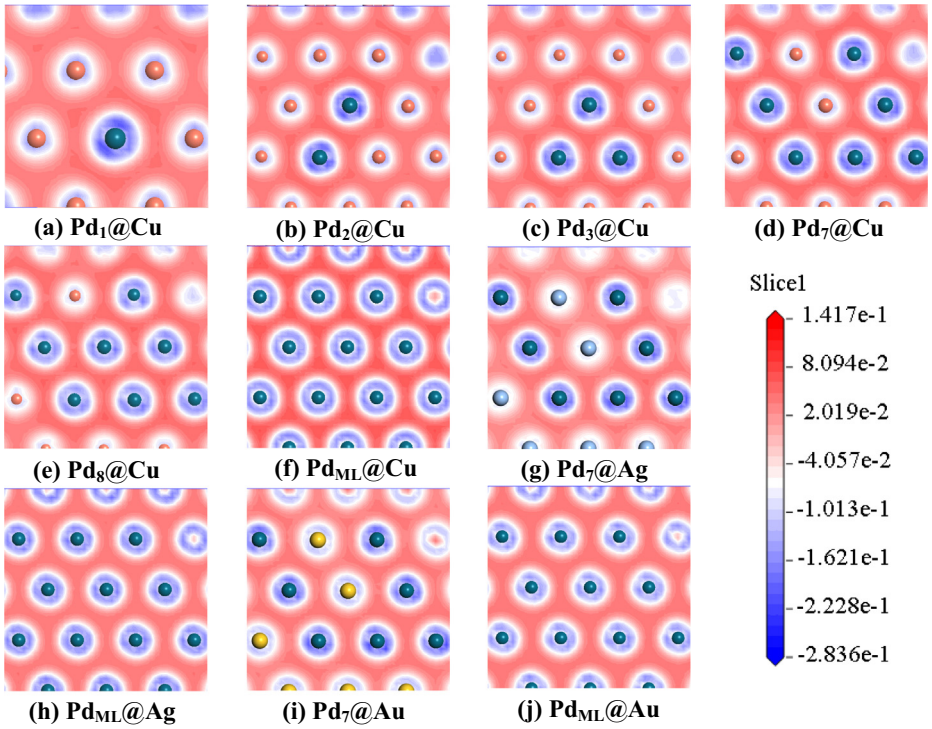

Fig. 7. Electron density difference contour maps of Pd@M (M = Cu, Ag, Au) alloy catalysts (a) Pd_1@Cu, (b) Pd_2@Cu, (c) Pd_3@Cu, (d) Pd_7@Cu, (e) Pd_8@Cu, (f) Pd_{ML}@Cu, (g) Pd_7@Ag, (h) Pd_{ML}@Ag, (i) Pd_7@Au, (j) Pd_{ML}@Au. Blue represents the electron depletion regions, and red represents the electron accumulation regions. (For interpretation of the references to color in this figure legend, the reader is referred to the web version of this article.)

(151.0 *vs.* 71.8, 47.8 kJ·mol^{-1}). Namely, for the same shell Pd ensemble consisted of dimer and trimer, the kinds of metal core obviously affect C_2H_4 selectivity and its formation activity.

As depicted in Fig. S12, the *d*-band center of Pd_7@M (M = Cu, Ag, Au) follows the order of Pd_7@Au (−3.496) < Pd_7@Ag (−3.374) < P d_7@Cu (−2.487), in which both Pd_7@Au and Pd_7@Ag shifts away compared to the Fermi level to present the lower C_2H_4 selectivity and its formation activity, whereas the *d*-band center of Pd_7@Cu stays near the Fermi level to exhibit the best catalytic performance. Moreover, as listed in Table 2, the average charge of the shell Pd atoms of Pd_7@Cu (0.847 *e*) is at the medium level compared to that of Pd_7@Ag and Pd_7@Au (0.958 and 0.999 *e*), thus, Pd_7@Cu presents the best catalytic performance toward C_2H_2 semi-hydrogenation.

Thus, C_2H_4 selectivity and its formation activity on the Pd_7@M (M = Cu, Ag, Au) catalysts also have a close relationship with the kinds of the metal core, taking C_2H_4 selectivity and its formation activity into account, Pd_7@Cu presents the best C_2H_4 selectivity (151.0 kJ·mol^{-1}) and its formation activity (5.66 × 10^6 s^{-1}·site^{-1}).

3.5.5. The influence of shell Pd ensemble in Pd@M (M = Cu, Ag, Au) on H_2 dissociation

Since H_2 dissociation is also the key step to provide hydrogen source for C_2H_2 semi-hydrogenation, as depicted in Fig. S13, H_2 dissociation was further investigated on the Pd@M (M = Cu, Ag, Au) catalysts, the results show that H_2 dissociation is much easier in kinetics on the Pd_1@Cu, Pd_2@Cu, Pd_3@Cu, Pd_7@Cu, Pd_8@Cu, Pd_{ML}@-Cu, Pd_7@Ag, Pd_{ML}@Ag, Pd_7@Au and Pd_{ML}@Au catalysts, the corresponding activation free energies are 36.6, 21.9, 25.6, 26.0, 32.9, 32.3, 23.1, 16.5, 27.6 and 15.5 kJ·mol^{-1}, respectively. Namely, Pd@M (M = Cu, Ag, Au) catalysts exhibit high catalytic activity toward H_2 dissociation into H atoms on these ten kinds of catalysts considered, which is not the rate-determining step of C_2H_2 semi-hydrogenation, and can provide enough hydrogen sources for C_2H_2 semi-hydrogenation.

3.5.6. The influence of Pd_7@M (M = Cu, Ag, Au) on green oil formation

As depicted is Fig. S5, for the polymerization process on Pd_7@Cu catalyst, the coupling of C_2H_2 + C_2H_3 to C_4H_5 is kinetically favorable among three coupling paths. However, starting from the adsorbed C_2H_3 species, the polymerization process via the coupling of C_2H_2 + C_2H_3 to C_4H_5 is more difficult in kinetics than C_2H_2 hydrogenation process via C_2H_4 desorption path (93.1 *vs.* 68.5 kJ·mol^{-1}). Thus, Pd_7@Cu catalyst not only favors the hydrogenation process to produce gas phase C_2H_4, but also effectively inhibits the polymerization process to form the green oil.

As depicted in Fig. S8, for Pd_7@Ag catalyst, beginning with the adsorbed C_2H_3 species, the hydrogenation process via C_2H_4 desorption path is energetically competitive with the polymerization process via the coupling route of C_2H_2 + C_2H_3 to C_4H_5 (83.3 *vs.* 85.3 kJ·mol^{-1}). Thus, different from Pd_7@Cu catalyst, Pd_7@Ag favors C_2H_2 semi-hydrogenation to form gas phase C_2H_4, however, the polymerization to form the green oil would affect the selectivity of gas phase C_2H_4. Similarly, as depicted in Fig. S10, for Pd_7@Au catalyst, the polymerization process via the coupling route of C_2H_2 + C_2H_3 to C_4H_5 is superior to its hydrogenation process via C_2H_4 desorption path (66.4 *vs.* 85.2 kJ·mol^{-1}), namely, Pd_7@Au easily produce green oil to deactivate the catalyst.

3.5.7. Microkinetic modeling on the Pd_7@M (M = Cu, Ag, Au) catalysts

Microkinetic modeling (Zhang et al., 2018; Gonçalves et al., 2020; Ayodele et al., 2020) is considered to probe into the catalytic activity and selectivity of C_2H_4 formation in C_2H_2 semi-hydrogenation on the Pd_7@M (M = Cu, Ag, Au) catalysts under typical experimental conditions (P_{C2H2} = 0.01 atm, P_{H2} = 0.1 atm, and T = 425 K). The results show that the reaction rate of C_2H_4 formation is 1.15 × 10^2 s^{-1}·site^{-1} and the relative selectivity of C_2H_4 is 100% on the Pd_7@Cu catalyst; meanwhile, those are 5.05 × 10^{-1} s^{-1}·site^{-1} and 100% on Pd_7@Ag, as well as 1.43 × 10^0 s^{-1}·site^{-1} and 100% on Pd_7@Au catalysts, suggesting that Pd_7@Cu catalyst

presents the highest activity of C_2H_4 formation (see details in the Supplementary Material), which agrees with the results obtained by the two-step model. Due to the impacts of surface species coverage, there is a certain degree of difference in the activity of C_2H_4 formation between two-step model and microkinetic modeling, however, both methods can be used to qualitatively and quantitatively judge C_2H_4 formation activity. Namely, the two-step model has a certain degree of rationality to determine C_2H_4 formation activity.

Overall, the catalytic performance of the core–shell Pd@M (M = Cu, Ag and Au) catalysts toward C_2H_2 semi-hydrogenation is closely related to the existence form of shell Pd ensemble, in which Pd_7@M catalysts with the shell Pd ensemble consisted of dimer and trimer exhibit the best C_2H_4 selectivity and its formation activity compared to Pd@M catalysts with other forms of shell Pd ensemble. On the other hand, among three kinds of Pd_7@M (M = Cu, Ag and Au) catalysts with the shell Pd ensemble of dimer and trimer, although both Pd_7@Au and Pd_7@Ag catalysts exhibit better C_2H_4 selectivity and its formation activity in the hydrogenation process, the green oil formation in the polymerization process is also easier than the gas phase C_2H_4 formation, namely, both Pd_7@Au and Pd_7@Ag catalysts are easily deactivated due to green oil formation. However, Pd_7@Cu not only favor C_2H_2 hydrogenation process to form gas phase C_2H_4 with the highest activity and selectivity, but also effectively inhibit the polymerization process to green oil that deactivate the catalysts, suggesting that Pd_7@Cu with the shell Pd ensemble consisted of dimer and trimer is a promising catalyst applied in C_2H_2 semi-hydrogenation.

Thus, it is proposed that the catalysts with the shell Pd ensemble of dimer and trimer can be also applied to other kinds of the core–shell catalysts consisted of the noble metal shell and the non-noble metal core in C_2H_2 semi-hydrogenation. Our study provides the valuable structure clue for the design of highly efficient core–shell catalyst consisted of the shell with the noble metal and the core with the non-noble metal; and it is believed that controlling the ensemble form of shell noble-metal may be a good way to adjust the catalytic performance toward the selective hydrogenation of other alkynes.

4. Conclusion

This study employed DFT and microkinetic modeling calculations to fully elucidate the mechanism of C_2H_2 semi-hydrogenation on the core–shell Pd_{shell}@Cu_{core} catalysts, aiming at revealing the influences of shell Pd ensemble form on C_2H_4 selectivity and its formation activity. Pd_1@Cu, Pd_2@Cu, Pd_3@Cu, Pd_7@Cu, Pd_8@Cu and Pd_{ML}@Cu were constructed to model Pd@Cu catalysts with different forms of shell Pd ensemble. Further, the obtained structure clues are applied to the Pd@Ag and Pd@Au catalysts to confirm the obtained structural information. The results showed that Pd_{ML}@Cu exhibits the lowest catalytic performance among the Pd@Cu catalysts; Pd_7@Cu catalyst with the shell Pd ensemble of dimer and trimer exhibits the best C_2H_4 selectivity and its formation activity. The same interesting results are also validated on the Pd_7@Ag and Pd_7@Au catalysts compared with other kinds of Pd@Ag and Pd@Au catalysts with different shell Pd ensembles. The analysis of electronic properties unveiled that the better catalytic performance of Pd_7@M (M = Cu, Ag, Au) with the shell Pd ensemble of dimer and trimer is ascribed to the moderate charge density and charge. Thus, adjusting the shell Pd ensemble of the core–shell alloy catalysts is an exceptional method to enhance the catalytic performance of gas phase C_2H_4 formation in C_2H_2 semi-hydrogenation.

CRediT authorship contribution statement

Yamin Qi: Writing - original draft, Writing - review & editing, Formal analysis. **Xiuxiu Shao:** Writing - original draft, Formal analysis. **Baojun Wang:** Writing - original draft, Writing - review & editing, Data curation, Conceptualization, Funding acquisition, Resources, Software, Project administration, Supervision. **Debao Li:** Formal analysis. **Lixia Ling:** Formal analysis. **Riguang Zhang:** Writing - original draft, Writing - review & editing, Data curation, Conceptualization, Funding acquisition, Resources.

Declaration of Competing Interest

The authors declare that they have no known competing financial interests or personal relationships that could have appeared to influence the work reported in this paper.

Acknowledgements

This work is financially supported by the National Natural Science Foundation of China (Nos. 21776193 and 22078221).

Appendix A. Supplementary material

The detailed descriptions about the activity of C_2H_4 formation on the Pd@M (M = Cu, Ag, Au), the calculation of the free energy, the effect of the unit cell size, the adsorption of H and C_2H_x(x = 2–5) species on the Pd@M (M = Ag, Au), C_2H_2 semi-hydrogenation on the Pd@M (M = Cu, Ag, Au), the *d*-band center, the projected density of states (*p*DOS) of Pd_7@M (M = Cu, Ag, Au) catalysts, H_2 dissociation on the Pd@M (M = Cu, Ag, Au) and microkinetic modeling on the Pd_7@M (M = Cu, Ag, Au) catalysts are presented. Supplementary data to this article can be found online at https://doi.org/10.1016/j.ces.2021.116941.

References

Ahn, I.Y., Lee, J.H., Kum, S.S., Moon, S.H., 2007. Formation of C4 species in the deactivation of a Pd/SiO_2 catalyst during the selective hydrogenation of acetylene. Catal. Today 123, 151–157.

Ando, F., Tanabe, T., Gunji, T., Kaneko, S., Takeda, T., Ohsaka, T., Matsumoto, F., 2018. Effect of the d-band center on the oxygen reduction reaction activity of electrochemically dealloyed ordered intermetallic platinum-lead (PtPb) nanoparticles supported on TiO_2-deposited cup-stacked carbon nanotubes. Appl. Nano Mater. 1, 2844–2850.

Ayodele, O.B., Cai, R.S., Wang, J.G., Ziouani, Y., Liang, Z.F., Spadaro, M.C., Kovnir, K., Arbiol, J., Akola, J., Palmer, R.E., Kolen'ko, Y.V., 2020. Synergistic computational-experimental discovery of highly selective PtCu nanocluster catalysts for acetylene semihydrogenation. ACS Catal. 10, 451–457.

Battiston, G.C., Dalloro, L., Tauszik, G.R., 1982. Performance and aging of catalysts for the selective hydrogenation of acetylene: a micropilot-plant study. Appl. Catal. 2, 1–17.

Brandt, K., Chiu, M.E., Watson, D.J., Tikhov, M.S., Lambert, R.M., 2009. Chemoselective catalytic hydrogenation of acrolein on Ag(111): effect of molecular orientation on reaction selectivity. J. Am. Chem. Soc. 131, 17286–17290.

Cao, X.M., Burch, R., Hardacre, C., Hu, P., 2011. An understanding of chemoselective hydrogenation on crotonaldehyde over Pt(111) in the free energy landscape: the microkinetics study based on first-principles calculations. Catal. Today 165, 71–79.

Cheng, J., Hu, P., Ellis, P., French, S., Kelly, G., Lok, C.M., 2008. Brønsted-evans-polanyi relation of multistep reactions and volcano curve in heterogeneous catalysis. J. Phys. Chem. C 112, 1308–1311.

Cheng, J., Hu, P., 2011. Theory of the kinetics of chemical potentials in heterogeneous catalysis. Angew. Chem. Int. Ed. 50, 7650–7654.

Cho, J.W., Lee, S., Yoon, S.P., Han, J., Nam, S.W., Lee, K.Y., Ham, H.C., 2017. Role of heteronuclear interactions in selective H_2 formation from HCOOH decomposition on bimetallic Pd/M (M=late transition FCC metal) catalysts. ACS Catal. 7, 2553–2562.

Choi, B.S., Song, J., Song, M.J., Goo, B.S., Lee, Y.W., Kim, Y., Yang, H., Han, S.W., 2019. Core-shell engineering of Pd-Ag bimetallic catalysts for efficient hydrogen production from formic acid decomposition. ACS Catal. 9, 819–826.

Delley, B., 1990. An all-electron numerical method for solving the local density functional for polyatomic molecules. J. Chem. Phys. 92, 508–517.

Delley, B., 1996. Fast calculation of electrostatics in crystals and large molecules. J. Phys. Chem. 100, 6107–6110.
Delley, B., 2000. From molecules to solids with the DMol^3 approach. J. Chem. Phys. 113, 7756–7764.
Deng, T., Cen, C., Shen, H.J., Wang, S.Y., Guo, J.D., Cai, S.H., Deng, M.S., 2020. Atom-pair catalysts supported by N-doped graphene for nitrogen reduction reaction: D-band center based descriptor. J. Phys. Chem. Lett. 11, 6320–6329.
Dolg, M., Wedig, U., Stoll, H., Preuss, H., 1987. Energy-adjusted ab initio pseudopotentials for the first row transition elements. J. Chem. Phys. 86, 866–872.
Duan, T., Zhang, R.G., Ling, L.X., Wang, B.J., 2016. Insights into the effect of Pt atomic ensemble on HCOOH oxidation over Pt-decorated Au bimetallic catalyst to maximize Pt utilization. J. Phys. Chem. C 120, 2234–2246.
Eren, B., Zherebetskyy, D., Patera, L.L., Wu, C.H., Bluhm, H., Africh, C., Wang, L.W., Somorjai, G.A., Salmeron, M., 2016. Activation of Cu(111) surface by decomposition into nanoclusters driven by CO adsorption. Science 351, 475–478.
Feng, X., Ling, L.X., Cao, Y.T., Zhang, R.G., Fan, M.H., Wang, B.J., 2018. A DFT study on the catalytic CO oxidative coupling to dimethyl oxalate on Al-doped core-shell Pd clusters. J. Phys. Chem. C 122, 1169–1179.
Friedrich, M., Villaseca, S.A., Szentmiklósi, L., Teschner, D., Armbrüster, M., 2013. Order-induced selectivity increase of $Cu_{60}Pd_{40}$ in the semi-hydrogenation of acetylene. Materials 6, 2958–2977.
Fu, W.W., Wang, Y.W., Tian, W., Zhang, H.J., Li, J., Wang, S.Y., Wang, Y., 2020. Non-metal single-phosphorus-atom catalysis of hydrogen evolution. Angew. Chem. Int. Ed. 59, 23791–23799.
Gonçalves, L.P.L., Wang, J.G., Vinati, S., Barborini, E., Wei, X.K., Heggen, M., Franco, M., Sousa, J.P.S., Petrovykh, D.Y., Soares, O.S.G.P., Kovnir, K., Akola, J., Kolen'ko, Y. V., 2020. Combined experimental and theoretical study of acetylene semi-hydrogenation over Pd/Al_2O_3. Int. J. Hydrogen. Energ. 45, 1283–1296.
Govind, N., Petersen, M., Fitzgerald, G., King-Smith, D., Andzelm, J., 2003. A generalized synchronous transit method for transition state location. Comp. Mater. Sci. 28, 250–258.
Guczi, L., Schay, Z., Stefler, G., Liotta, L.F., Deganello, G., Venezia, A.M., 1999. Pumice-supported Cu-Pd catalysts: influence of copper on the activity and selectivity of palladium in the hydrogenation of phenylacetylene and but-1-ene. J. Catal. 182, 456–462.
Halgren, T.A., Lipscomb, W.N., 1977. The synchronous-transit method for determining reaction pathways and locating molecular transition states. Chem. Phys. Lett. 49, 225–232.
He, F., Li, K., Xie, G.Y., Wang, Y., Jiao, M.G., Tang, H., 2016. Understanding the enhanced catalytic activity of $Cu_1@Pd_3(111)$ in formic acid dissociation, a theoretical perspective. J. Power Source 316, 8–16.
Hook, A., Celik, F.E., 2017. Predicting selectivity for ethane dehydrogenation and coke formation pathways over model Pt-M surface alloys with ab initio and scaling method. J. Phys. Chem. C 121, 17882–17892.
Huang, W., McCormick, J.R., Lobo, R.F., Chen, J.G., 2007. Selective hydrogenation of acetylene in the presence of ethylene on zeolite-supported bimetallic catalysts. J. Catal. 246, 40–51.
Khan, N.A., Shaikhutdinov, S., Freund, H.J., 2006. Acetylene and ethylene hydrogenation on alumina supported Pd-Ag model catalysts. Catal. Lett. 108, 159–164.
Komeili, S., Ravanchi, M.T., Taeb, A., 2015. The influence of alumina phases on the performance of the $Pd-Ag/Al_2O_3$ catalyst in tail-end selective hydrogenation of acetylene. Appl. Catal. A-Gen. 502, 287–296.
Krajčí, M., Hafner, J., 2014. Selective semi-hydrogenation of acetylene: atomistic scenario for reactions on the polar threefold surfaces of GaPd. J. Catal. 312, 232–248.
Lee, J.H., Kim, S.K., Ahn, I.Y., Kim, W.J., Moon, S.H., 2011. Performance of $Pd-Ag/Al_2O_3$ catalysts prepared by the selective deposition of Ag onto Pd in acetylene hydrogenation. Catal. Commun. 12, 1251–1254.
Lee, J.H., Cho, J.W., Jeon, M., Ridwan, M., Park, H.S., Choi, S.H., Nam, S.W., Han, J., Lim, T.H., Ham, H.C., Yoon, C.W., 2016. Experimental and computational studies of formic acid dehydrogenation over PdAu: influence of ensemble and ligand effects on catalysis. J. Mater. Chem. A 4, 14141–14147.
Leviness, S., Nair, V., Weiss, A.H., Schay, Z., Guczi, L., 1984. Acetylene hydrogenation selectivity control on $PdCu/Al_2O_3$ catalysts. J. Mol. Catal. 25, 131–140.
Liu, D., 2016. DFT study of selective hydrogenation of acetylene to ethylene on Pd doping Ag nanoclusters. Appl. Surf. Sci. 386, 125–137.
Liu, H.Y., Wang, B.J., Fan, M.H., Henson, N., Zhang, Y.L., Towler, B.F., Harris, H.G., 2013. Study on carbon deposition associated with catalytic CH_4 reforming by using density functional theory. Fuel 113, 712–718.
Lu, L., Shen, L.P., Shi, Y., Chen, T.T., Jiang, G.Q., Ge, C.W., Tang, Y.W., Chen, Y., Lu, T.H., 2012. New insights into enhanced electrocatalytic performance of carbon supported Pd-Cu catalyst for formic acid oxidation. Electrochim. Acta 85, 187–194.
Ma, L.L., Lv, C.Q., Wang, G.C., 2017. A DFT study and micro-kinetic analysis of acetylene selective hydrogenation on Pd-doped Cu(111) surfaces. Appl. Surf. Sci. 410, 154–165.
Ma, H.Y., Wang, G.C., 2020. Selective hydrogenation of acetylene on Pt_n/TiO_2 (n=1, 2, 4, 8) surfaces: Structure sensitivity analysis. ACS Catal. 10, 4922–4928.
McCue, A.J., McRitchie, C.J., Shepherd, A.M., Anderson, J.A., 2014. Cu/Al_2O_3 catalysts modified with Pd for selective acetylene hydrogenation. J. Catal. 319, 127–135.
McCue, A.J., Guerrero-Ruiz, A., Rodríguez-Ramos, I., Anderson, J.A., 2016. Palladium sulphide-A highly selective catalyst for the gas phase hydrogenation of alkynes to alkenes. J. Catal. 340, 10–16.
Meier, L.A., Castellani, N.J., 2017. Theoretical study of Sn adsorbed on the Au(111) surface. Comp. Mater. Sci. 127, 48–59.
Meng, L.D., Wang, G.C., 2014. A DFT+U study of acetylene selective hydrogenation over anatase supported Pd_aAg_b(a+b=4) cluster. Phys. Chem. Chem. Phys. 16, 17541–17550.
Ngamsom, B., Bogdanchikova, N., Borja, M.A., Praserthdam, P., 2004. Characterisations of $Pd-Ag/Al_2O_3$ catalysts for selective acetylene hydrogenation: effect of pretreatment with NO and N_2O. Catal. Commun. 5, 243–248.
Osswald, J., Kovnir, K., Armbrüster, M., Giedigkeit, R., Jentoft, R.E., Wild, U., Grin, Y., Schlögl, R., 2008. Palladium-gallium intermetallic compounds for the selective hydrogenation of acetylene: Part II: surface characterization and catalytic performance. J. Catal. 258, 219–227.
Paul, J.F., Sautet, P., 1994. Influence of the surface atom metallic coordination in the adsorption of ethylene on a platinum surface: a theoretical study. J. Phys. Chem. 98, 10906–10912.
Pei, G.X., Liu, X.Y., Wang, A., Lee, A.F., Isaacs, M.A., Li, L., Pan, X.L., Yang, X.F., Wang, X. D., Tai, Z.J., Wilson, K., Zhang, T., 2015. Ag alloyed Pd single-atom catalysts for efficient selective hydrogenation of acetylene to ethylene in excess ethylene. ACS Catal. 5, 3717–3725.
Ren, M.J., Zhou, Y., Tao, F.F., Zou, Z.Q., Akins, D.L., Yang, H., 2014. Controllable modification of the electronic structure of carbon-supported core-shell Cu@Pd catalysts for formic acid oxidation. J. Phys. Chem. C 118, 12669–12675.
Sárkány, A., Horváth, A., Beck, A., 2002. Hydrogenation of acetylene over low loaded Pd and $Pd-Au/SiO_2$ catalysts. Appl. Catal. A-Gen. 229, 117–125.
Sárkány, A., Geszti, O., Sáfrán, G., 2008. Preparation of Pd_{shell}-Au_{core}/SiO_2 catalyst and catalytic activity for acetylene hydrogenation. Appl. Catal. A-Gen. 350, 157–163.
Song, Q.Q., Li, J.Q., Wang, S.L., Liu, J.L., Liu, X.X., Pang, L.Y., Li, H., Liu, H., 2019. Enhanced electrocatalytic performance through body enrichment of Co-based bimetallic nanoparticles in situ embedded porous N-doped carbon spheres. Small 15, 1903395.
Takht, R.M., Fadaeerayeni, S., Rahimi Fard, M., 2014. An egg-shell $Pd-Ag/\alpha-Al_2O_3$ catalyst for tail-end acetylene selective hydrogenation. Iran. J. Chem. Eng. 11, 42–54.
Tedsree, K., Li, T., Jones, S., Chan, C.W.A., Yu, K.M.K., Bagot, P.A.J., Marquis, E.A., Smith, G.D.W., Tsang, S.C.E., 2011. Hydrogen production from formic acid decomposition at room temperature using a Ag-Pd core-shell nanocatalyst. Nat. Nanotechnol. 6, 302–307.
Tian, D.X., Zhang, H.L., Zhao, J.J., 2007. Structure and structural evolution of Ag_n(n=3-22) clusters using a genetic algorithm and density functional theory method. Solid State Commun. 144, 174–179.
Vincent, M.J., Gonzalez, R.D., 2004. Selective hydrogenation of acetylene through a short contact time reactor. AIChE J. 48, 1257–1267.
Wang, Y.X., Cao, L., Libretto, N.J., Li, X., Li, C.Y., Wan, Y.D., He, C., Lee, J.S., Gregg, J., Zong, H., Su, D., Miller, J.T., Mueller, T., Wang, C., 2019. Ensemble effect in bimetallic electrocatalysts for CO_2 reduction. J. Am. Chem. Soc. 141, 16635–16642.
Wang, Y., Wang, B.J., Ling, L.X., Zhang, R.G., Fan, M.H., 2020. Probe into the effects of surface composition and ensemble effect of active sites on the catalytic performance of C_2H_2 semi-hydrogenation over the Pd-Ag bimetallic catalysts. Chem. Eng. Sci. 218, 115549–115561.
Wang, Z.L., Yan, J.M., Wang, H.L., Ping, Y., Jiang, Q., 2013. Au@Pd core-shell nanoclusters growing on nitrogen doped mildly reduced graphene oxide with enhanced catalytic performance for hydrogen generation from formic acid. J. Mater. Chem. A 1, 12721–12725.
Wehrli, J.T., Thomas, D.J., Wainwright, M.S., Trimm, D.L., Cant, N.W., 1991. Reduced foulant formation during the selective hydrogenation of C2, C3, and C4 acetylenes. Stud. Surf. Sci. Catal. 68, 203–210.
Xu, L., Stangland, E.E., Mavrikakis, M., 2018. Ethylene versus ethane: a DFT-based selectivity descriptor for efficient catalyst screening. J. Catal. 362, 18–24.
Yang, B., Burch, R., Hardacre, C., Headdock, G., Hu, P., 2012. Origin of the increase of activity and selectivity of nickel doped by Au, Ag, and Cu for acetylene hydrogenation. ACS Catal. 2, 1027–1032.
Yang, B., Burch, R., Hardacre, C., Headdock, G., Hu, P., 2013. Influence of surface structures, subsurface carbon and hydrogen, and surface alloying on the activity and selectivity of acetylene hydrogenation on Pd surfaces: a density functional theory study. J. Catal. 305, 264–276.
Yang, B., Burch, R., Hardacre, C., Headdock, G., Hu, P., 2014. Understanding the optimal adsorption energies for catalyst screening in heterogeneous catalysis. ACS Catal. 4, 182–186.
Yang, B., Burch, R., Hardacre, C., Hu, P., Hughes, P., 2014. Selective hydrogenation of acetylene over Pd-Boron catalysts: a density functional theory study. J. Phys. Chem. C 118, 3664–3671.
Yang, B., Burch, R., Hardacre, C., Hu, P., Hughes, P., 2016. Importance of surface carbide formation on the activity and selectivity of Pd surfaces in the selective hydrogenation of acetylene. Surf. Sci. 646, 45–49.
Yang, B., Burch, R., Hardacre, C., Hu, P., Hughes, P., 2017. Selective hydrogenation of acetylene over Cu(211), Ag(211) and Au(211): Horiuti-Polanyi mechanism vs. non-Horiuti-Polanyi mechanism. Catal. Sci. Technol. 2, 1508–1514.
Yang, J., Lv, C.Q., Guo, Y., Wang, G.C., 2012. A DFT+U study of acetylene selective hydrogenation on oxygen defective anatase (101) and rutile (110) TiO_2 supported Pd_4 cluster. J. Chem. Phys. 136, 104107.
Yang, J.Q., Shi, L., Liu, X., Wen, Y.W., Cho, K., Zhao, Y.K., Chen, R., Shan, B., 2019. Unravelling origins of Pd ensembles' activity in CO oxidation via state-to-state microkinetic analysis. J. Catal. 371, 276–286.

Yuan, D.W., Liu, Z.R., 2013. Atomic ensemble effects on formic acid oxidation on PdAu electrode studied by first-principles calculations. J. Power Sources 224, 241–249.
Zhang, Y.Y., Diao, W.J., Williams, C.T., Monnier, J.R., 2014. Selective hydrogenation of acetylene in excess ethylene using Ag- and Au-Pd/SiO_2 bimetallic catalysts prepared by electroless deposition. Appl. Catal. A-Gen. 469, 419–426.
Zhang, J., Sui, Z.J., Zhu, Y.A., Chen, D., Zhou, X.G., Yuan, W.K., 2016. Composition of the green oil in hydrogenation of acetylene over a commercial Pd-Ag/Al_2O_3 catalyst. Chem. Eng. Technol. 39, 865–873.
Zhang, R.G., Zhao, B., Ling, L.X., Wang, A.J., Russell, C.K., Wang, B.J., Fan, M.H., 2018. Cost-effective palladium-doped Cu bimetallic materials to tune selectivity and activity by using doped atom ensembles as active sites for efficient removal of acetylene from ethylene. ChemCatChem 10, 2424–2432.
Zhang, R.G., Zhao, B., He, L.L., Wang, A.J., Wang, B.J., 2018. Cost-effective promoter-doped Cu-based bimetallic catalysts for the selective hydrogenation of C_2H_2 to C_2H_4: the effect of the promoter on selectivity and activity. Phys. Chem. Chem. Phys. 20, 17487–17496.
Zhao, J.B., Zha, S.J., Mu, R., Zhao, Z.J., Gong, J.L., 2018. Coverage effect on the activity of the acetylene semihydrogenation over Pd-Sn catalysts: a density functional theory study. J. Phys. Chem. C 122, 6005–6013.
Zhao, Z.J., Zhao, J.B., Chan, X., Zha, S.J., Zeng, L., Gong, J.L., 2019. Competition of C-C bond formation and C-H bond formation for acetylene hydrogenation on transition metals: a density functional theory study. AIChE J. 65, 1059–1066.
Zhao, Y., Zhu, M.Y., Kang, L.H., 2018. The DFT study of single-atom Pd_1/g-C_3N_4 catalyst for selective acetylene hydrogenation reaction. Catal. Lett. 148, 2992–3002.
Zhou, C.G., Wu, J.P., Nie, A., Forrey, R.C., Tachibana, A., Cheng, H.S., 2007. On the sequential hydrogen dissociative chemisorption on small platinum clusters: a density functional theory study. J. Phys. Chem. C 111, 12773–12778.